Available online at www.sciencedirect.com
ScienceDirect
Journal of Catalysis 250 (2007) 350–359
JOURNAL OF CATALYSIS
www.elsevier.com/locate/jcat

Direct propylene epoxidation over barium-promoted Au/Ti-TUD catalysts with H_2 and O_2: Effect of Au particle size

Jiqing Lu [a,b], Xiaoming Zhang [a,c], Juan J. Bravo-Suárez [a], Kyoko K. Bando [a], Tadahiro Fujitani [a], S. Ted Oyama [a,d,*]

[a] *Research Institute for Innovation in Sustainable Chemistry, National Institute of Advanced Industrial Science and Technology, AIST Tsukuba West, 16-1 Onogawa, Tsukuba, Ibaraki 305-8569, Japan*

[b] *Zhejiang Key Laboratory for Reactive Chemistry on Solid Surfaces, Institute of Physical Chemistry, Zhejiang Normal University, Jinhua 321004, PR China*

[c] *Chengdu Institute of Organic Chemistry, Chinese Academy of Sciences, Chengdu 610041, PR China*

[d] *Environmental Catalysis and Nanomaterials Laboratory, Department of Chemical Engineering (0211), Virginia Polytechnic Institute and State University, Blacksburg, VA 24061, USA*

Received 7 February 2007; revised 7 June 2007; accepted 7 June 2007

Available online 6 August 2007

Abstract

A catalyst consisting of gold supported on a Ti-containing silicate mesoporous material (TUD) with 13-nm pores was used for the epoxidation of propylene with mixtures of H_2 and O_2. The catalyst activity was enhanced by the addition of a Ba promoter. The pH of deposition was important in controlling the gold loading and particle size. A pH of 7 gave a Au loading of 2.7 wt% and an average particle size of 2.0 nm, as determined by transmission electron microscopy, whereas a pH of 9 produced a much lower Au loading of 0.11 wt% and smaller particles of size about 0.9 nm, as estimated by X-ray absorption fine structure measurements. At 423 K and 0.1 MPa total pressure, the catalyst prepared at pH 7 gave a steady-state propylene conversion of 2.1%, a propylene oxide (PO) selectivity of 79%, and a H_2 efficiency of 3.8%, whereas that prepared at pH 9 gave a conversion of 1.4%, a PO selectivity of 99%, and a H_2 efficiency of 17%. The turnover frequency for PO production based on total gold increased on going to the sample prepared at pH 9. Thus, it is concluded that very small Au particles (about 1 nm) are the most active for epoxidation, whereas larger Au particles (about 2 nm) are less active because they promote direct H_2 oxidation to H_2O. X-ray absorption near-edge spectroscopy results indicated that at reaction conditions, the small particles had partially oxidized gold but the larger particles had metallic gold, suggesting that the smaller particles had high coverage of oxygen or oxygen-derived species.

Keywords: Propylene; Epoxidation; Gold; Nanoparticle

1. Introduction

Propylene oxide (PO) is an important chemical intermediate used in the production of polyurethane, polyester resins, and surfactants. Commercially, PO is produced by the chlorohydrin process and several organic hydroperoxide processes [1], but these processes suffer from deficiencies. The chlorohydrin process produces large amounts of byproduct salts and chlorinated organic compounds, whereas the hydroperoxide processes produce stoichiometric quantities of co-products that have lower commercial value than PO (e.g., *t*-butylalcohol and styrene) or must be recycled (e.g., cumene). Although supported silver catalysts are used for ethylene epoxidation with molecular oxygen, the direct epoxidation of propylene with molecular oxygen on these catalysts has low selectivity because the allylic hydrogens in propylene are reactive and their abstraction by surface oxygen species leads to total combustion products [2–6].

Recently, several companies, such as Lyondell and Bayer [7], BASF, Solvay and Dow [8], and Degussa, Headwaters, and Krupp Uhde [9] have announced the development of liquid-phase processes for the epoxidation of propylene catalyzed by titanium silicalite-1 (TS-1) using H_2O_2. Although these processes do not produce byproducts or co-products, the H_2O_2

* Corresponding author.
E-mail address: oyama@vt.edu (S.T. Oyama).

0021-9517/$ – see front matter
doi:10.1016/j.jcat.2007.06.006

is expensive, and research on the use of mixtures of H_2 and O_2 for propylene epoxidation has attracted considerable attention.

Catalysts that have been investigated for simultaneous H_2O_2 formation and propylene epoxidation include palladium or palladium/platinum supported on titanium silicalite [10–14] and gold supported on titania [15,16] and on various titanosilicates, including Ti-MCM-41, Ti-MCM-48, TS-1, TS-2, and Ti-β [17–22]. Recently, two groups have reported Au catalysts supported on Ti-containing materials with high activity. The group of Haruta reported a Ba-promoted Au catalyst supported on a three-dimensional mesoporous titanosilicate that gave an initial PO formation rate of 92 $g_{PO}\,h^{-1}\,kg_{cat}^{-1}$ [23,24]. Unfortunately, the catalyst suffered from quick deactivation over a span of 4 h, but the deactivation could be suppressed appreciably by adding trimethylamine in the feed stream as a gas-phase promoter [25]. The group of Delgass focused on Au supported on the microporous titanosilicate TS-1 [26–29], which they found to be very stable and active. One of their catalysts, a 0.05 wt% Au/TS-1 (Si/Ti = 36), gave a propylene conversion of 8.8% and a PO selectivity of 81% at 473 K, corresponding to a PO formation rate of 116 $g_{PO}\,h^{-1}\,kg_{cat}^{-1}$ [29]. Three important points should be made concerning the conversion of propylene. First, the value of 8.8% reported by Delgass et al. [29] is extremely high; most studies have reported quasi-steady-state conversions of 1–2% [30]. Second, the overwhelming majority of studies have encountered deactivation, with conversion levels deteriorating over 2–6 h. Third, in the area of propylene epoxidation, the target conversion level for commercialization is about 10%, similar to that obtained in ethylene epoxidation over silver catalysts [31].

It is commonly believed that the Au particles have a critical effect on the catalytic performance [32]. Haruta et al. [15] inferred that Au particles 2–5 nm in size are responsible for epoxidation, whereas particles smaller than 2 nm are responsible for hydrogenation to form propane. However, Delgass et al. [29] suggested that Au particles smaller than 2 nm could contribute significantly to epoxidation, based on the fact that Au particles could not be observed by transmission electron microscopy (TEM) on their Au/TS-1 catalysts. They also performed density functional theory (DFT) calculations and found that three atom gold clusters could form hydrogen peroxide, suggesting that small clusters also could be active for PO formation [33]. The discrepancy may be due to the use of a bulk TiO_2 support by Haruta et al. [15] and of a microporous support with highly dispersed Ti(IV) species by Delgass et al. [29].

In this paper, we report the direct propylene epoxidation on gold promoted by Ba on a mesoporous titanosilicate support (Ti–TUD). The catalyst produces a low propylene conversion level of 1.4% but is stable, which makes it amenable to further study. For example, we have recently used it for a study of the kinetics of the reaction [34], where a power-rate law expression, $r_{PO} = k(H_2)^{0.54}(O_2)^{0.24}(C_3H_6)^{0.36}$, was found. Here we examined the effect of Au particle size on PO and H_2O formation and found that particles around 1 nm gave the best performance. EXAFS analysis of the catalysts under reaction conditions revealed that the active catalyst contains some partially oxidized Au species.

2. Experimental

2.1. Catalyst preparation

The Ti–TUD support with Ti/Si = 3/100 was prepared by a modified sol–gel method similar to that reported by Maschmeyer et al. [35]. In a typical preparation, 14.7 g of tetraethylammonium hydroxide solution (TEAOH, 20% aqueous solution, Merck) was added dropwise to a mixture of 1.02 g of tetrabutylorthotitanate (TBOT, TCI, 99.0%) and 20.8 g of tetraethylorthosilicate (TEOS, Wako, 95.0%) at 273 K under vigorous stirring. After continuously stirring for 1 h at room temperature, a clear yellow solution was obtained. Then, 19.8 g of H_2O was added dropwise, and the stirring was continued for another 1 h. The clear solution was transferred into a Teflon-lined autoclave and aged statically at 373 K for 3 h. Finally, 29.8 g of triethanolamine (TEA, Wako, 98.0%) was added dropwise under vigorous stirring. The final homogeneous mixture, with a molar composition of 1 SiO_2:0.03 TiO_2:0.2 TEAOH:2 TEA:17.5 H_2O, was stirred at room temperature for 24 h, dried at 373 K for 24 h, heated in air to 973 K at a ramp rate of 1 K min^{-1}, and calcined at that temperature for 10 h. A similar method was used to prepare the pure silicon sample, Si–TUD, in which the titanium component was excluded from the synthesis mixture.

The Ti–TUD-supported Au catalysts were prepared using a deposition–precipitation (DP) method [36]. In a typical preparation, 100 ml of 2.4 mM $HAuCl_4{\cdot}4H_2O$ solution ($HAuCl_4{\cdot}4H_2O$, WAKO, 99.0%) was heated to 343 K under vigorous stirring. The pH of the solution was adjusted to 8.9 using a 1 M Na_2CO_3 solution. After this, 1 g of the support was added, and the suspension was stirred for 15 min. Then 0.19 mmol of $Ba(NO_3)_2$ (Chamelon Reagent, 99.0%) dissolved in 5 ml H_2O was added, and the mixture was stirred for another 45 min at the same temperature and pH. The solid was filtered and washed with 100 ml of Millipore H_2O (Autopure WEX 3, Yamato, relative conductivity >15 MΩ cm), dried under vacuum for 12 h, and then calcined in air at 573 K for 4 h. The sample was designated Au–Ba/Ti–TUD (9), where the number in parentheses refers to the final pH during preparation. A similar procedure was used to prepare samples at different pH or samples without the addition of the barium salt. For the Au supported on Si–TUD catalyst, preparation was done as described previously [16].

2.2. Characterization

Surface area, pore volume, and pore size distribution of the support were measured in a volumetric adsorption unit (Micromeritics ASAP 2020). TEM images of the Au catalysts were obtained in a microscope (Hitachi H-9000) operated at 300 kV. Particle size distributions were obtained by measuring the diameters of about 200 particles in a representative region. The content of Au, Ba, and Ti in the catalysts was determined by inductively coupled plasma analysis, whereas the content of Cl was measured by X-ray fluorescence spectrometry (Rigaku ZSX mini). Ammonia temperature-programmed desorption (NH_3-TPD) measurements were conducted on a flow

unit (BEL-CAT). Before measurements, the sample was heated in He (30 $cm^3\ min^{-1}$) at 373 K for 2 h to remove water. The adsorption amount was calculated by comparing NH_3 desorption peak areas with calibration NH_3 pulses of a known volume.

The ultraviolet-visible (UV–vis) spectrum of the support was collected using a large-compartment spectrometer (Varian Cary 5000) equipped with a praying mantis diffuse reflectance attachment (DRP-XXX), using $BaSO_4$ as the reference.

In situ X-ray absorption fine structure (XAFS) measurements were carried out at beamlines BL7C and BL9A of the Photon Factory in the Institute of Materials Structure Science, High-Energy Accelerator Research Organization (PF-IMSS-KEK) in Japan. All the spectra were obtained in transmission mode using an in situ XAFS cell provided with a flow delivery system. All of the reaction conditions, including temperature, pressure, and gas flow rate, could be monitored and controlled from outside of the radiation shield hutch. XAFS spectra were obtained about every 10 min in a step-scanning mode under the same pretreatment and reaction conditions as used in the catalytic testing reactor. Analysis of extended X-ray absorption fine structure (EXAFS) and X-ray absorption near-edge structure (XANES) data was conducted with commercially available software (REX, Rigaku). Parameters for backscattering amplitudes and phase-shift functions were extracted from the oscillations of standard substances (Au foil) obtained at reaction temperatures to account for thermal fluctuations. Other reference standards used were $AuPPh_3Cl$ for Au(I) and $HAuCl_4$ for Au(III). These air-sensitive materials were pressed into wafers and sealed in polyethylene in a glove box.

2.3. Catalytic testing

The epoxidation of propylene was carried out in a quartz tubular microreactor (6 mm I.D., 180 mm long) using 0.3 g of catalyst of 100–140 mesh size without dilution. The reactor was equipped with an axial quartz thermocouple well (2 mm O.D.), which allowed monitoring of the catalyst bed temperature. The respective flow rates of Ar (99.9%), O_2 (99.5%), H_2 (99.5%), and C_3H_6 (99.8%) were 24.5, 3.5, 3.5, and 3.5 $cm^3\ min^{-1}$ and were controlled by mass flow meters, with the reaction pressure set at 0.1 MPa. The space velocity was 7000 $cm^3\ h^{-1}\ g_{cat}^{-1}$. Before reaction, the catalyst was pretreated with a mixture of 10 vol% H_2 in Ar (27 $cm^3\ min^{-1}$), followed by 10 vol% O_2 in Ar (27 $cm^3\ min^{-1}$) at 523 K for 0.5 h, after which the temperature was set to 423 K under Ar flow and the reactants were introduced. The same pretreatment steps were also used for the XAFS experiments and are shown in detail in Scheme 1. For the latter measurements, He was used as the inert gas, because Ar has stronger absorption of X-rays.

Reaction products were analyzed online using two gas chromatographs (Shimadzu GC-14), each equipped with a flame ionization detector (FID) and a thermal conductivity detector (TCD). One had a FFAP capillary column (0.32 mm × 60 m) and a Porapak Q compact column (3 mm × 2 m), and the other had a MS-5A 60/80 compact column (3 mm × 2 m) and a Gaskuropak 54 84/100 compact column (3 mm × 2 m). The FFAP capillary column and Porapak Q were used to detect

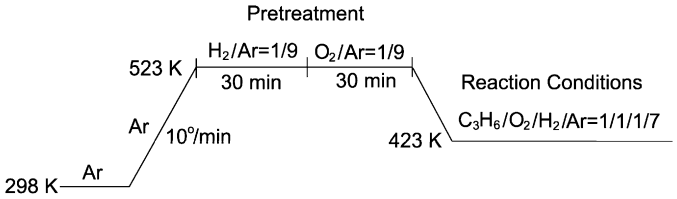

Scheme 1. Pretreatment of samples.

oxygenates (i.e., acetaldehyde, PO, acetone, propionaldehyde, acrolein, acetic acid, and isopropanol) and CO_2 and H_2O, respectively, whereas the MS-5A and Gaskuropak columns were used to analyze H_2, O_2, and CO and hydrocarbons (propane, propylene, ethylene and ethane), respectively. Carbon balances were close to 100 ± 3%. Because the major products observed were propylene oxide (C_3H_6O), CO_2, and H_2O, the reactions occurring on the catalysts were taken to be

$$C_3H_6 + H_2 + O_2 \rightarrow C_3H_6O + H_2O,$$

$$C_3H_6 + 9/2O_2 \rightarrow 3CO_2 + 3H_2O,$$

and

$$H_2 + 1/2O_2 \rightarrow H_2O.$$

Based on these reactions, the propylene conversion, PO selectivity, H_2 conversion, and H_2 efficiency (also known as H_2 selectivity) were defined as follows:

Propylene conversion = mol of (oxygenates + $CO_2/3$)/mol of propylene in feed.

PO selectivity = mol of PO/mol of (oxygenates + $CO_2/3$).

H_2 conversion = mol of H_2 reacted/moles of H_2 in feed.

H_2 efficiency = mol of PO/moles of H_2O.

3. Results

The nitrogen adsorption–desorption analysis of the Ti–TUD support is shown in Fig. 1. The BET surface area of the support was 501 $m^2\ g^{-1}$, and the pore volume was 1.32 $cm^3\ g^{-1}$. The surface area was lower than that of a related material reported

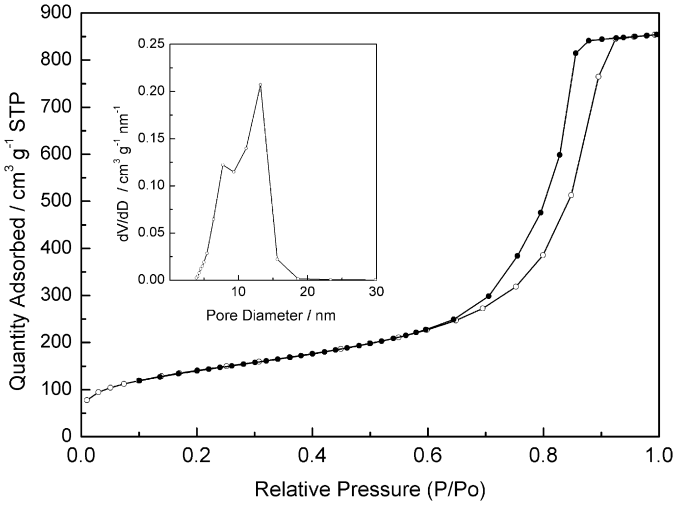

Fig. 1. N_2 adsorption–desorption isotherm and pore size distribution of Ti–TUD support.

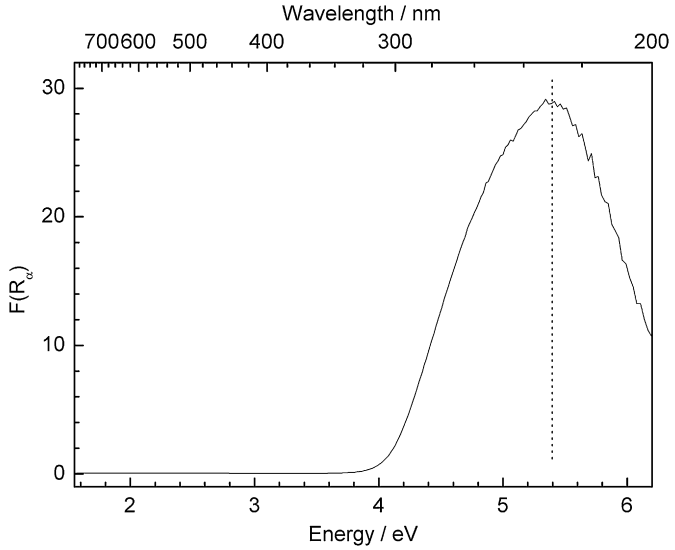

Fig. 2. UV–vis spectrum of Ti–TUD support.

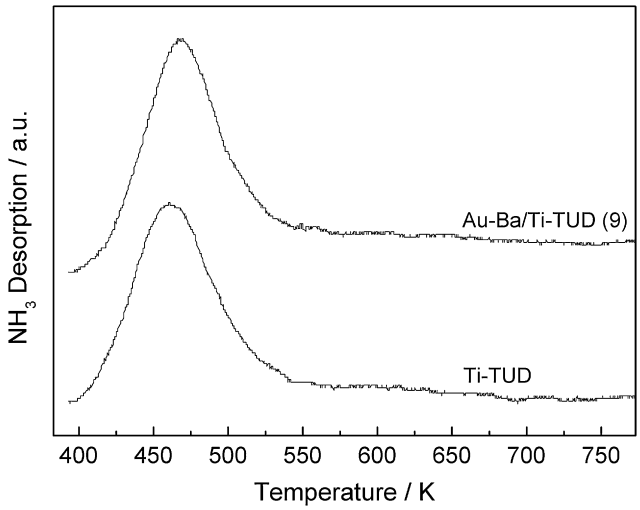

Fig. 3. Ammonia temperature-programmed desorption (TPD) for Ti–TUD and Au–Ba/Ti–TUD (9).

Table 1
Actual metal loadings of Au–Ba/Ti–TUD catalysts prepared at different pH values

Catalyst name	Final pH	Ti content (wt%)	Au loading (wt%)	Ba loading (wt%)	Cl content (wt%)[b]	D_p (nm)
Au/Si–TUD (9)	9	0	∼1	0	Zero	3.9
Ba/Ti–TUD (9)	8.9	2.2	0	2.5	Zero	–
Au–Ba/Ti–TUD (7)	6.8	2.2	2.70	1.3	Zero	2.0
Au–Ba/Ti–TUD (9)	8.9	2.2	0.11	2.4	Zero	0.9[c]
Au–Ba/Ti–TUD (10)	10.0	2.2	0.09	2.4	Zero	NM
Au/Ti–TUD (9)	8.9	2.2	0.07	0	Zero	NM
Au–Ba/Ti–TUD (7)[a]	7.0	2.2	1.7	NM	NM	2.5

NM: not measured.
[a] The catalyst was neutralized using 0.1 M NaOH solution at pH 7.
[b] Determined by X-ray fluorescence spectroscopy (XRF).
[c] Average particle diameter estimated by extended X-ray absorption fine structure (EXAFS).

by Haruta et al. [24], whereas the pore volume was similar. The support exhibited a type IV isotherm, which is characteristic of a mesoporous material. The insert of Fig. 1 shows the pore size distribution curve, centered at 13 nm, with a shoulder at 8 nm.

Fig. 2 presents the UV–vis spectrum of the Ti–TUD support. A broad band at 230 nm is shown, characteristic of tetrahedrally coordinated Ti(IV) species in the silica matrix [37–39]. The increased width of this band has been attributed to a distorted tetrahedral coordination environment [37]. A shoulder at 260–270 nm indicates the presence of Ti(IV) species in 5- or 6-fold coordination, which could be generated through hydration of the tetrahedrally coordinated Ti(IV) species [40,41]. The absence of a band above 330 nm implies that extra-framework titania was not present.

Table 1 shows metal loadings of the catalysts prepared at different pH values using the DP method. A Ti content in the catalyst of 2.2 wt% closely corresponds to the Ti/Si molar ratio (3/100) used in the synthesis of the support. The actual Au loading changed dramatically with the pH used during the DP process. The Au loading decreased with increasing pH values, from 2.7 wt% at pH 7 to 0.09 wt% at pH 10. The Ba loadings in the Au–Ba/Ti–TUD catalysts prepared at pH 9 and 10 were 2.4 wt%, meaning that almost all of the Ba^{2+} in the initial solution was deposited on the support, probably in the form of $BaCO_3$ precipitates as Na_2CO_3 was used at high pH. In the Au–Ba/Ti–TUD catalyst prepared at pH 7, the Ba content was lower (1.3 wt%), possibly due to the relatively neutral environment in the solution. The table also summarizes the results of gold particle size determinations by TEM and EXAFS, which we discuss later.

Fig. 3 shows NH_3–TPD measurements for the Ti–TUD support and the Au–Ba/Ti–TUD (9) catalyst. Integration of the desorption areas and comparison with pulses of pure NH_3 reveals that the Ti–TUD support adsorbed 0.234 mmol g^{-1}, whereas the Au–Ba/Ti–TUD (9) catalyst adsorbed 0.218 mmol g^{-1}.

Fig. 4 shows TEM images of Au–Ba/Ti–TUD (7) and Au–Ba/Ti–TUD (9), and a particle size histogram for Au–Ba/Ti–TUD (7). The Au–Ba/Ti–TUD (7) catalyst has numerous Au particles and a narrow particle size distribution centered at 2 nm. The Au–Ba/Ti–TUD (9) catalyst, however, shows no Au particles larger than 1 nm, which is close to the instrumental resolution. This may be due to the extremely low Au content and to the formation of very small particles at the pH at which this sample was prepared. The TEM image of the Au–Ba/Ti–TUD (7) neutralized with NaOH (not shown) reveals a similar Au particle size distribution as that neutralized with Na_2CO_3, namely homogeneously distributed Au particles of about 2 nm.

Table 2 summarizes the catalytic activities of the catalysts at steady state. In most cases, the main products were PO and CO_2 with trace amounts of acetone and acrolein. A catalyst without Ti (Au/Si–TUD (9)) and a catalyst without Au (Ba/Ti–TUD (9)) were largely inactive for epoxidation, indicating that both Ti and Au species are necessary for high activity. For the Au/Ti–TUD catalysts, it can be seen that the promotion of the catalyst with barium enhanced the activity. Propylene conversion increased from 0.9 to 1.4% after Ba promotion on the Au/Ti–TUD (9) catalyst. Increasing the pH of preparation from 7 to 9 and to 10 decreased the propylene conversion but significantly increased the PO selectivity. Furthermore, catalysts prepared at

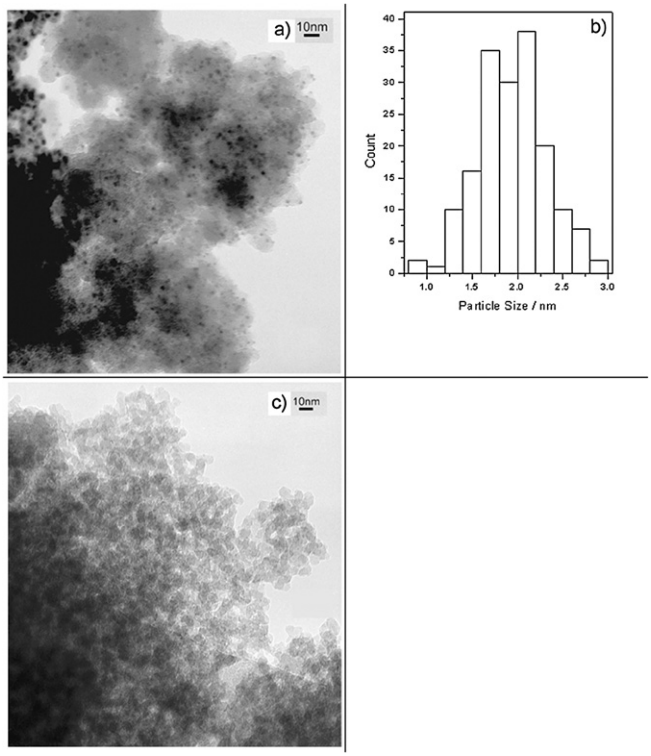

Fig. 4. Transmission electron microscopy (TEM) images of catalysts. (a) Au–Ba/Ti–TUD (7) catalyst before reaction, (b) particle size distribution of Au–Ba/Ti–TUD (7) catalyst before reaction, (c) Au–Ba/Ti–TUD (9) catalyst before reaction.

pH 7 using a different neutralizing agent, such as NaOH or Na_2CO_3, exhibited similar catalytic behavior, indicating that neutralizing agents have little effect on the catalysts. It is also interesting to note that on the catalysts prepared at pH 7 using either NaOH or Na_2CO_3 the H_2 conversions are much higher than those prepared at pH 9 or 10. Because these Au–Ba/Ti–TUD (7) catalysts have lower PO selectivity, the H_2 efficiency was much lower than that on the Au–Ba/Ti–TUD (9) catalyst. The table also reports turnover frequencies (TOFs) based on total gold content. The TOF increases in going from the sample prepared at pH 7–9, but then decreases for the sample prepared at pH 10.

Fig. 5 shows the reactivity of the samples prepared at pH 7, 9, and 10. The order of reactivity was Au–Ba/Ti–TUD (7) > Au–Ba/Ti–TUD (9) > Au–Ba/Ti–TUD (10) (Fig. 5a). For all of the catalysts, propylene conversion decreased with time but reached steady state in about 5–6 h. Loss of initial activity is common in supported Au catalysts [21–24], possibly due to the oligomerization of PO on the surface [42]. As for the PO selectivity, the catalysts prepared at pH 9 and 10 showed extremely high PO selectivity (almost 100%), whereas the catalyst prepared at pH 7 showed a substantially lower value (77%) at steady state (Fig. 5b). H_2 conversion on the samples prepared at pH 9 and 10 was low, about 5% at steady state, whereas that of the sample prepared at pH 7 was close to 50% (Fig. 5c). Correspondingly, H_2 efficiencies of the samples prepared at pH 9 and 10 were 17 and 20%, respectively, compared with 2.5% for the sample prepared at pH 7 (Fig. 5d).

Fig. 6 shows the changes in the Au L_{III}-edge XANES, normalized to the same edge jump, observed for the Au–Ba/Ti–TUD (9) and the Au–Ba/Ti–TUD (7) catalysts under reaction conditions. The Au foil exhibits three near-edge features at 11,934, 11,946, and 11,968 eV, which are characteristic of Au(0). For the Au–Ba/Ti–TUD (7) catalyst, there were three peaks at 11,937, 11,950, and 11,973 eV, which also can be attributed to Au(0). The shift of the peaks to higher energy is due to the smaller Au particle size in the catalyst [43]. A weak white line peak at 11,923 eV indicates that some oxidized Au species was present in the fresh sample; however, this peak disappeared after pretreatment. Moreover, EXAFS analysis of Fig. 6f gave Au–Au distances (coordination number (CN) = 7.9, (R) = 0.282 nm), which also confirmed the presence of metallic Au clusters. For the Au–Ba/Ti–TUD (9) catalyst, the spectra were noisy because of the low Au content, and the white line peak at 11,923 eV can be attributed to either Au(I) or Au(III) [43–45]. The intensity of the peak decreased slightly, suggesting that some oxidized Au species were reduced during pretreatment. But this oxidized Au species was still present during the reaction. Therefore, it is clear that the Au–Ba/Ti–TUD (9) catalyst contained some amount of partially oxidized Au species, whereas the Au–Ba/Ti–TUD (7) catalyst contained almost all reduced Au.

EXAFS analysis of the catalysts was carried out to determine the CNs of the metal atoms and thus calculate the particle sizes of the Au clusters. Fig. 7 shows measurements of the Au–Ba/Ti–TUD (7) catalyst carried out at in situ reaction conditions and those of the Au–Ba/Ti–TUD (9) catalyst carried out after reaction (due to equipment malfunction). The figure

Table 2
Propylene epoxidation on Au/Ti–TUD catalysts prepared at different pH values

Catalysts	Conversion (%)			PO sel. (%)	PO formation rate		H_2 effic. (%)
	C_3H_6	O_2	H_2		($g_{PO}\ h^{-1}\ kg_{cat}^{-1}$)	($TOF = mol_{PO}\ s^{-1}\ mol_{Au}^{-1}$)	
Au/Si–TUD (9)	0.2	32.1	59.4	19.4	0.7	0.00007	0.1
Ba/Ti–TUD (9)	0	0	0	0	0.0	0	0
Au–Ba/Ti–TUD (7)	2.1	24.5	51.9	76.8	29.2	0.0011	3.8
Au–Ba/Ti–TUD (9)	1.4	2.5	4.9	99.6	25.3	0.0217	17.2
Au–Ba/Ti–TUD (10)	0.8	1.6	3.2	99.5	14.4	0.0151	18.8
Au/Ti–TUD (9)	0.9	3.2	4.7	99.0	16.1	0.0218	17.4
Au–Ba/Ti–TUD (7)[a]	2.1	27.0	49.5	75.2	28.6	0.0016	2.8

Reaction temperature: 423 K.
[a] The catalyst was neutralized using 1 M NaOH solution at pH 7.

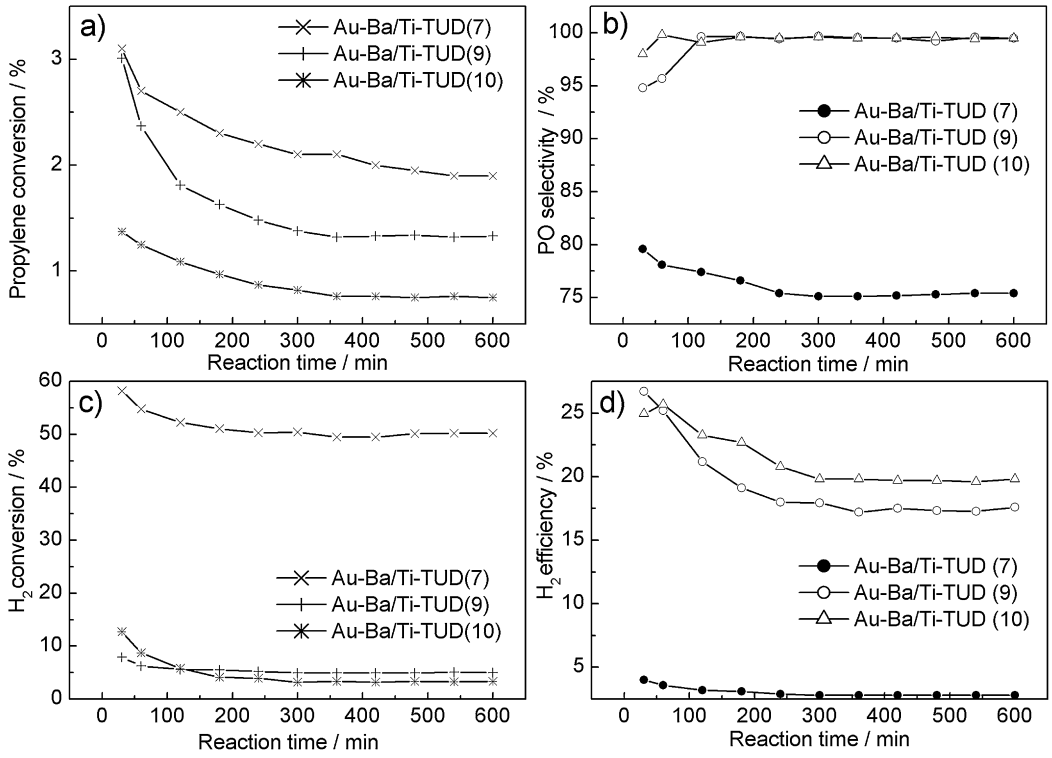

Fig. 5. Propylene epoxidation on the Au–Ba/Ti–TUD (7), Au–Ba/Ti–TUD (9), and Au–Ba/Ti–TUD (10) catalysts. (a) Propylene conversion, (b) PO selectivity, (c) H_2 conversion, (d) H_2 efficiency. Reaction conditions: $C_3H_6/O_2/H_2/Ar = 3.5/3.5/3.5/24.5$ cm^3 min^{-1}, S.V. = 7000 cm^3 h^{-1} g$_{cat}^{-1}$, $T = 423$ K, $P = 0.1$ MPa.

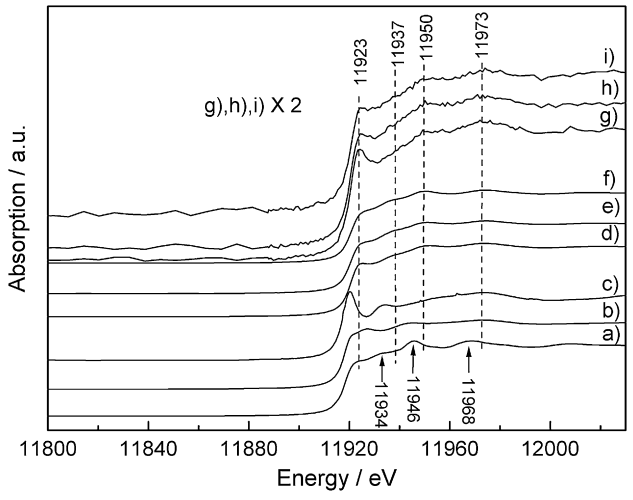

Fig. 6. Au L_{III}-edge XANES spectra observed for (a) Au foil, (b) Au(I)PPh_3-Cl, (c) HAu(III)Cl_4, (d) Au–Ba/Ti–TUD (7) fresh catalyst under He at 298 K, (e) Au–Ba/Ti–TUD (7) under He at 423 K, after H_2 and O_2 pretreatment, (f) Au–Ba/Ti–TUD (7) under PO reaction conditions at 423 K after 6 h, (g) Au–Ba/Ti–TUD (9) fresh catalyst under He at 298 K, (h) Au–Ba/Ti–TUD (9) under He at 423 K, after H_2 and O_2 pretreatment, (i) Au–Ba/Ti–TUD (9) under PO reaction conditions at 423 K after 6 h.

summarizes the raw data (Figs. 7a and 7b), the Fourier transforms (Figs. 7c and 7d), and the curve fitting results (Figs. 7d and 7e). It was verified that the XANES spectra of the sample were identical during and after the reaction. The results, summarized in Table 3, show CNs of 7.9 for Au–Ba/Ti–TUD (7) and 6.9 for Au–Ba/Ti–TUD (9). Assuming spherical particles and using models of fcc Au clusters, the mean particle sizes for the Au–Ba/Ti–TUD (7) and Au–Ba/Ti–TUD (9) samples are calculated as 1.4 and 0.9 nm, respectively [46–48]. The correlation reported by Bond and Thompson of gold particle size and dispersion gives dispersion values of about 85% for Au–Ba/Ti–TUD (7) and 95% for Au–Ba/Ti–TUD (9) [49].

4. Discussion

Ti–TUD with a surface area of 501 m^2 g^{-1} was synthesized in this work and used as a support for Au catalysts. The predominant pore size of the material was 13 nm, and the material can be considered a mesoporous solid (Fig. 1). UV–vis characterization of the support showed that it contained Ti(IV) species in tetrahedral coordination (Fig. 2). This has been reported to be beneficial for the direct propylene epoxidation with H_2 and O_2 [26].

A series of Au–Ba/Ti–TUD catalysts were prepared at various pH values using the DP method. The Au loadings measured by ICP analysis tracked the preparation pH (Table 1), with lower pH values favoring higher gold deposition on the support. Barium content increased slightly at higher pH, as was expected for the precipitation of barium carbonate. No traces of chlorine were detected on the catalysts, indicating that the washing procedure effectively removed the chlorine.

The catalyst promoted with Ba (Au–Ba/Ti–TUD (9)) gave higher propylene conversion than the unpromoted catalyst (Au/Ti–TUD (9)) (Table 2). The use of Ba in this work was motivated by the report that it enhanced activity [23,25]. However, the previous studies did not attempt to ascertain the role

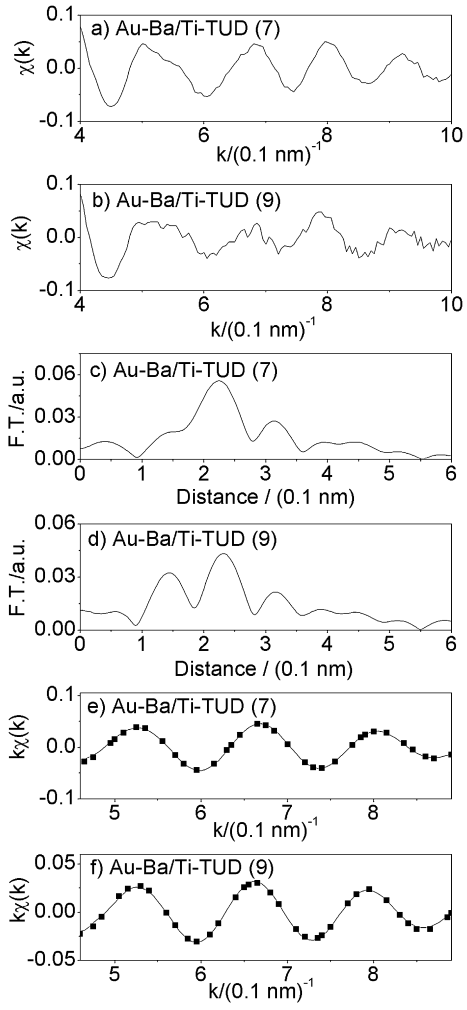

Fig. 7. EXAFS analysis of Au–Ba/Ti–TUD (7): (a, c, e) and Au–Ba/Ti–TUD (9): (b, d, f) (a, b) raw EXAFS $\chi(k)$; (c, d) Fourier transforms; (e, f) curve fitting results, points are observed, lines are calculated.

Table 3
EXAFS analysis of the Au–Ba/Ti–TUD (7) and Au–Ba/Ti–TUD (9) catalysts

Catalyst	Bond	CN	d (nm)	ΔE_0 (eV)	σ (nm)	R (%)	D (nm)
Au–Ba/Ti–TUD (7)	Au–Au	7.9	0.282	0.45	0.0083	0.05	1.4
Au–Ba/Ti–TUD (9)[a]	Au–Au	6.9	0.281	−5.0	0.090	1.07	0.9
	Au–O	0.94	0.198	−7.9	0.068	2.6	

CN: coordination number, d: nearest-neighbor distance, ΔE_0: energy difference between a reference, σ: Debye–Waller factor, R: $100 \times (\sum(\chi_{obs} - \chi_{cal})^2 / \sum \chi_{obs}^2)^{1/2}$, where where χ represents a normalized EXAFS oscillation, D: particle size (from coordination number).

[a] For this analysis, empirical parameters Au–Au $R = 0.2884$ nm (extracted from Au foil) and Au–O $R = 0.20$ nm (extracted from Au_2O_3) are used.

of Ba. One study speculated that Ba promoted the formation of hydroperoxide species from H_2 and O_2 and neutralized acid sites on the catalyst surface, but gave no evidence for these hypotheses [25]. In this work we evaluated the acidity of the Ti–TUD support and the Au–Ba/Ti–TUD (9) catalyst by ammonia TPD measurements (Fig. 3). The two materials were found to have similar NH_3 adsorption amounts (0.234 and 0.218 mmol g^{-1}, respectively), indicating that the effect of Ba is not to reduce acidity. Elemental analysis showed that Ba increases the amount of gold retained by the catalyst by 50% (Table 1), accounting for the improved propylene conversion in the promoted catalyst.

The TEM images show that numerous Au particles with a mean diameter of 2 nm are present on the Au–Ba/Ti–TUD (7) catalyst (Figs. 4a and 4b), whereas Au particles could not be observed for Au–Ba/Ti–TUD (9) (Fig. 4c). Because the resolution of the instrument was about 1 nm, this finding does not rule out the presence of smaller particles; indeed, as discussed later, EXAFS results demonstrate Au particles of about 0.9 nm in the latter sample. These findings are consistent with the results of Moreau et al. [50], who investigated the effect of pH on Au/TiO_2 catalysts during a deposition precipitation process and found that Au particles deposited at pH 7 were larger than those deposited at pH 9. They suggested that this was partly because the surface was more positively charged and attracted more gold anionic species at low pH. Moreover, at low pH, more chloride remained on the catalyst, leading to Au particle agglomeration. In our study, we detected no chlorine in the samples, and the increase in Au particle size for Au–Ba/Ti–TUD (7) was likely due to its much higher Au content (2.70 wt%) compared with that of Au–Ba/Ti–TUD (9) (0.11 wt%), which caused the formation of larger Au clusters during calcination.

Typical results for reactivity on these catalysts show an initial decline in the conversion over the first 2–3 h, along with an increase in selectivity (Fig. 5). The activity lined out after 6 h and remained constant thereafter. Propylene conversion decreased, but selectivity increased, as the pH of the catalyst preparation was increased from 7 to 9 and then to 10 (Table 2). We discuss this finding later.

Delgass et al. [28] compared various neutralizing agents on Au/TS-1 catalysts, including Na_2CO_3 and KOH, and found that Na_2CO_3 gave the best results, whereas Haruta et al. [22] claimed that NaOH as a neutralizing agent gave the best catalytic performance. The two catalysts prepared at pH 7 neutralized by either NaOH or Na_2CO_3 showed comparable performance (Table 2), indicating that in this case, the neutralizing agent had little effect on the catalytic activity. They gave rise to a similar Au loading and particle size distribution on both catalysts.

The activity of the catalysts is summarized in Table 2, which lists reactant conversions, PO selectivity, hydrogen efficiency, and two PO formation rates. The first PO rate is a specific rate or yield (per kg of catalyst) in units that are commonly used in ethylene and propylene epoxidation. The second PO rate is an effective TOF based on total Au, not corrected for dispersion, which in any case is very high. The catalytic performance of the Au–Ba/Ti–TUD (9) was comparable to that obtained by Sinha et al. [24], who used a gold catalyst supported on a similar Ti-containing three-dimensional mesoporous material. We found that the specific catalytic activity (per kg of catalyst) of the Au–Ba/Ti–TUD catalysts decreased as the pH of preparation was raised from 7 to 9 and then to 10 (Table 2, column 6). However, the effective TOF (TOF = $mol_{PO}\, s^{-1}\, mol_{Au}^{-1}$) first increased as the pH was raised from 7 to 9, and then decreased as the pH was further raised to 10 (Table 2, column 7). This can be explained by the gold component, as we discuss below.

Table 4
Oxidation state of gold in the catalysts before and during reaction[a]

Catalyst	State	Au(0)/Au(I)	Au(0)/Au(III)
Au–Ba/Ti–TUD (7)	Calcined	68/32	84/16
Au–Ba/Ti–TUD (7)	During reaction	100/0	100/0
Au–Ba/Ti–TUD (9)	Calcined	29/71	53/47
Au–Ba/Ti–TUD (9)	During reaction	63/37	70/30

[a] From XANES alone it could not be determined if oxidized gold was either Au(I) or Au(III). Calcined: fresh catalyst under He at 298 K. During reaction: under PO reaction conditions at 423 K after 6 h.

Several points should be emphasized before we discuss the role of gold. First, the gold content decreased with increasing pH (Table 1). The reason for this has been well explained by Moreau et al. [50]; during synthesis, the Au anion complexes are increasingly repelled from the more negatively charged surface of the support at higher pH. Second, as shown by our TEM and EXAFS data, the size of the gold particles decreased with decreasing gold content as the pH of preparation increased. Third, gold is believed to form hydrogen peroxide, which then migrates to Ti sites to carry out the epoxidation reaction [15,16,22,26,28,29]. Finally, it has been reported by Barton and Podkolzin [51] that gold clusters of 0.7 nm (corresponding to Au_{13} clusters) are the most active for hydrogen oxidation, producing the highest amount of an intermediate *OOH hydroperoxide. Smaller particles are purportedly less reactive due to the instability of the *OOH intermediate, whereas larger particles are purportedly less reactive due to the instability of adsorbed oxygen. Returning to the discussion of gold, our findings are in accordance with the results of Barton and Podkolzin [51]. The increase in TOF in going from the Au–Ba/Ti–TUD (7) to the Au–Ba/Ti–TUD (9) sample is hypothesized to be due to the decrease in size of the gold particles from 2 to 0.9 nm, consistent with results from DFT calculations [51]. These smaller gold sizes produce more hydroperoxide. The subsequent decrease in TOF in going to the Au–Ba/Ti–TUD (10) sample is likely due to a further decrease in the size of the gold clusters, which according to Barton and Podkolzin [51] decreases their ability to form hydroperoxides.

The XANES results show that compared with Au–Ba/Ti–TUD (7), the Au–Ba/Ti–TUD (9) catalyst contained some oxidized Au components under reaction conditions (Fig. 6). The higher state of oxidation of the fine gold particles is consistent with the theoretical results of Barton and Podkolzin [51] demonstrating that larger gold particles do not chemisorb oxygen strongly. Pattern fitting analysis of Au L_{III}-edge XANES was used to estimate the amounts of Au(0) and Au(I) or Au(III) in the catalysts before and during reaction. The results are summarized in Table 4. Note that the fitting of the Au(I) and Au(III) references gave similar results, and we could not determine whether the gold existed as Au(I) or Au(III) in the catalyst samples. This has been reported by others; for example, Benfield et al. [43], Fernandez et al. [44], and Salama et al. [45] showed that it is difficult to distinguish between the edge positions of different oxidation states of gold including Au(0), Au(I), and Au(III). Although Cunningham et al. [52] reported a difference in edge position between Au(0) and Au(III), with the latter giving a lower edge energy, in general XANES spectral features are deemed more reliable for establishing the oxidation state. Because of the low signal levels in our work, it is difficult to be certain of the oxidation state; Table 4 gives both values. Yet, the general results are very clear. For the Au–Ba/Ti–TUD (7) catalyst in the calcined state, a substantial amount of the gold was in metallic form, with either 32% Au(I) or 16% Au(III), whereas during reaction, the gold was predominantly in the metallic state. For the Au–Ba/Ti–TUD (9) catalyst in the calcined state, the proportion of oxidized gold was much higher, with either 71% Au(I) or 47% Au(III), and this oxidized gold was retained during reaction with either 37% Au(I) or 30% Au(III). Oxidized gold species have been reported earlier for highly dispersed samples and in fact have been suggested to be the active centers for the CO oxidation reaction [53]. It also has been suggested that the perimeter of gold nanoclusters may be especially active for the activation of oxygen [54,55]. The structure of the gold phase for the catalysts in this study cannot be established conclusively. The XANES results are consistent with any number of possible arrangements, such as the oxidized gold being on the outside of a core-and-shell structure or in the peripheral region of an interfacial oxide layer. However, the reactivity results for the Au–Ba/Ti–TUD (7) sample indicate that metallic gold is associated with significant hydrogen combustion (Table 2).

It should be noted that the oxidation of the smaller clusters is an intrinsic property of gold and has been observed before by others, including Miller et al. [56] and Radnik et al. [57]. It does not have to do with the Ba, which is likely in the form of a carbonate and is relatively neutral. XANES measurements of Au–Ba/Ti–TUD (9) and Au/Ti–TUD (9) (not shown) indicate no charging of the gold due to Ba.

The EXAFS results for the Au–Ba/Ti–TUD (7) and Au–Ba/Ti–TUD (9) samples are presented in Fig. 7. The raw data (Figs. 7a and 7b) of the sample prepared at pH 9 show considerable more noise than that of the sample prepared at pH 7 because of the former sample's much lower gold concentration (Table 1). The Fourier transforms (Figs. 7c and 7d) show distinct peaks that can be assigned to Au–Au distances in both samples and, in the case of the sample prepared at pH 9, a peak assignable to Au–O [56]. The curve-fitting results show good agreement between measured and calculated values (Figs. 7e and 7f). EXAFS analysis has been used effectively to determine metal particle sizes [47,48,56]. Analysis of the samples after reaction (Table 3) indicates that the particle sizes of the gold clusters are 1.4 nm for the Au–Ba/Ti–TUD (7) sample and 0.9 nm for the Au–Ba/Ti–TUD (9) sample. This is in reasonable agreement with the TEM results. The distinct Au–O peak seen in the sample prepared at pH 9 with the smaller particle size is indicative of oxidation and agrees with the XANES results (Fig. 6). We also found that the Au–Au distance in the smaller particles was slightly less than that in the larger particles. This agrees with the findings of Miller et al. [56], who studied a large number of supported gold samples, and also with a more limited study by Radnik et al. [57]. The decrease in distance is not as large as that found in the previous investigations, but this can be explained by the presence of the oxygen in the smaller gold

particles, which would tend to expand the gold–gold distance by formation of Au–O–Au bridges.

Haruta and collaborators earlier found that Au particles 2–5 nm in diameter are effective for propylene epoxidation [15,24], whereas Au particles smaller than 2 nm produce propane [15]. The latter result was obtained on a TiO_2 support, where the particle shape is hemispherical. However, Delgass et al. concluded that Au particles smaller than 2 nm also could be involved in epoxidation, as supported by their catalytic results on Au/TS-1 [26] and their DFT calculations on a 3-atom gold cluster [33]. Our findings support the conclusion that small Au particles that could not be observed by TEM, but whose presence and particle size (0.9 nm) could be determined by EXAFS [sample Au–Ba/Ti–TUD (9)], are particularly active for epoxidation. Smaller particle sizes, such as those likely found in the sample prepared at pH 10, are less effective for PO production.

The conversion of H_2 was much higher on the Au–Ba/Ti–TUD (7) catalyst than on the Au–Ba/Ti–TUD (9) (Table 2 and Fig. 5). An explanation for this is that there are sites on larger gold particles that carry out hydrogen oxidation to H_2O. These are likely to be the surface gold atoms on the larger particles that are not in the periphery of the particles close to Ti atoms in the support. Other results showed that Au particles of around 2 nm are very active for H_2 oxidation [58]. Smaller gold particles would have smaller quantities of these nonperipheral sites and thus a lower propensity to combust hydrogen. It has been shown that Au particles tend to interact with Ti(IV) [59] and that Au loading tracks the Ti content of the catalysts [29].

On the Au–Ba/Ti–TUD (9) catalyst, the Au content was 5.6 $\mu mol\, g^{-1}$ and the Ti content was 476 $\mu mol\, g^{-1}$, about a hundred-fold difference. Because there are about 28 Au atoms in a 0.9-nm Au particle and the dispersion is about 95% [49], there should have been sufficient Ti sites next to each Au cluster. The slight activity difference for PO formation between the Au–Ba/Ti–TUD (9) and Au–Ba/Ti–TUD (7) catalysts is likely due to the Ti sites in proximity to Au, whereas the large selectivity difference is due to the difference in Au sizes between the two catalysts, because the oxygen species adsorbed on the large Au particles oxidize PO to CO_2 and H_2O.

It is believed that epoxidation occurs at or close to the interface of Au–Ti sites, where the hydrogen peroxide formed on the Au site can transfer to the Ti(IV) sites and form titanium hydroperoxide species and react with propylene [15,60]. On the larger Au particles, the formed hydrogen peroxide cannot move to Ti sites because of the longer distance, and these hydrogen peroxide species decompose to H_2O or are involved in nonselective oxidation. Indeed, this is the case when the PO reaction is carried out over a Au/Si–TUD (9) catalyst, which resulted in a large H_2 conversion (about 60%) mostly generating H_2O, and producing only 19% PO (Table 2). The remainder of 81% of CO_2 indicates that the Au is carrying out complete combustion. Also, as observed from the effective TOF ($mol_{PO}\, s^{-1}\, mol_{Au}^{-1}$) in Table 2, the contribution to PO formation due to reaction on gold particles is very small [Au/Si–TUD (9) vs Au–Ba/Ti–TUD (9)]. Barton and Podkolzin [51] proposed that water formation over Au nanoparticles proceeds through the formation of *OOH intermediates, which can react with hydrogen to form H_2O. A fraction of these hydroperoxo intermediates could be responsible for the small amount of PO produced by the Au/Si–TUD catalyst. A catalyst without gold, Ba/Ti–TUD (9) is completely inactive for PO formation (Table 2) indicating that both Au and Ti are required for high selectivity and activity in propylene oxidation with H_2 and O_2.

5. Conclusions

A stable and active catalyst for the epoxidation of propylene with mixtures of H_2 and O_2 was prepared by the deposition–precipitation of gold onto a Ti-containing mesoporous substrate (Ti–TUD). The activity of the catalyst was enhanced by the addition of a Ba promoter, which increased the gold loading but had no effect on the acidity of the catalyst. The pH of deposition was important in controlling the gold loading and particle size. A pH of 7 gave a Au loading of 2.7 wt% and particles of 2.0 nm average size (85% dispersion); a pH of 9 produced a much lower Au loading of 0.11 wt% and smaller particles, about 0.9 nm (95% dispersion); and a pH of 10 further decreased the Au loading to 0.09 wt%. Selectivity to PO increased with increasing pH of preparation. The effective turnover rate for PO formation based on total gold was a maximum for the sample prepared at pH 9, indicating that gold particles around 1 nm in size were optimal for the epoxidation reaction. This may be associated with a preferred size for hydrogen peroxide formation from H_2 and O_2. Higher H_2 conversion was found on the high-Au loading catalyst prepared at pH 7, suggesting that larger Au nanoparticles were responsible for H_2 combustion. XANES results at reaction conditions for the sample prepared at pH 9 indicated that the active Au species on the catalyst were partially oxidized, whereas the sample prepared at pH 7 had metallic Au.

Acknowledgments

Financial support was provided by the Japanese Ministry of Economy, Trade and Industry (METI, Minimum Energy Chemistry Project) and the National Science Foundation (grant CBET 0651238). J.J.B.-S. and S.T.O. acknowledge financial support from the Japan Society for the Promotion of Science (JSPS) through the postdoctoral fellowship for foreign researcher program (P05627) and the invited fellow program. The authors also thank Mr. T. Arai (ETRI, AIST) for assistance with the XRF measurements and Ms. M. Makino for the TEM measurements. The XAFS experiments were conducted under approval of PF-PAC (proposals 2004G304 and 2006G362).

References

[1] K. Weissermel, H.J. Arpe, Industrial Organic Chemistry, second ed., VCH, New York, 1993, pp. 141, 264.
[2] M.A. Barteau, R.J. Madix, J. Am. Chem. Soc. 105 (1983) 344.
[3] M. Akimoto, K. Ichikawa, E. Echigoya, J. Catal. 76 (1982) 333.
[4] J.T. Roberts, R.J. Madix, W.W. Crew, J. Catal. 141 (1993) 300.
[5] J.Q. Lu, J.J. Bravo-Suárez, A. Takahashi, M. Haruta, S.T. Oyama, J. Catal. 232 (2005) 85.
[6] J.Q. Lu, J.J. Bravo-Suárez, M. Haruta, S.T. Oyama, Appl. Catal. A 302 (2006) 283.

[7] Hydrocarbon Process. 83 (5) (2004) 35.
[8] Chemical & Engineering News, News of the Week, September 6, 2004, p. 15.
[9] Chemical & Engineering News, Business Concentrates, May 27, 2002. p. 19.
[10] A. Sato, T. Miyake, Japan Patent 4,352,771, December 7, 1992, to Tosoh.
[11] A. Sato, M. Oguri, M. Tokumaru, T. Miyake, Japan Patent Appl. 269,029, October 15, 1996, to Tosoh.
[12] A. Sato, M. Oguri, M. Tokumaru, T. Miyake, Japan Patent Appl. 269,030, October 15, 1996, to Tosoh.
[13] M. Fisher, P. Lingelbach, U. Muller, N. Rieber, P. Bassler, J. Dembowski, K. Eller, W. Harder, V. Kohl, German Patent Appl. DE 44 25 672 Al, January 25, 1996, to BASF AG.
[14] R. Meiers, U. Dingerdissen, W.F. Hölderich, J. Catal. 176 (1998) 376.
[15] T. Hayashi, K. Tanaka, M. Haruta, J. Catal. 178 (1998) 566.
[16] T.A. Nijhuis, T. Visser, B.M. Weckhuysen, J. Phys. Chem. B 109 (2005) 19309.
[17] M. Haruta, B.S. Uphade, S. Tsubota, A. Miyamoto, Res. Chem. Intermed. 24 (1998) 329.
[18] Y.A. Kalvachev, T. Hayashi, S. Tsubota, M. Haruta, J. Catal. 186 (1999) 228.
[19] B.S. Uphade, M. Okumura, S. Tsubota, M. Haruta, Appl. Catal. A 190 (2000) 43.
[20] T.A. Nijhuis, B.J. Huizinga, M. Makkee, J.A. Moulijn, Ind. Eng. Chem. Res. 38 (1999) 884.
[21] B.S. Uphade, Y. Yamada, T. Akita, T. Nakamura, M. Haruta, Appl. Catal. A 215 (2001) 137.
[22] B.S. Uphade, T. Akita, T. Nakamura, M. Haruta, J. Catal. 209 (2002) 331.
[23] A.K. Sinha, S. Seelan, S. Tsubota, M. Haruta, Angew. Chem. Int. Ed. 43 (2004) 1546.
[24] A.K. Sinha, S. Seelan, M. Okumura, T. Akita, S. Tsubota, M. Haruta, J. Phys. Chem. B 109 (2005) 3956.
[25] B. Chowdhury, J.J. Bravo-Suárez, M. Daté, S. Tsubota, M. Haruta, Angew. Chem. Int. Ed. 45 (2006) 412.
[26] N. Yap, R.P. Andres, W.N. Delgass, J. Catal. 226 (2004) 156.
[27] L. Cumaranatunge, W.N. Delgass, J. Catal. 232 (2005) 38.
[28] E.E. Stangland, B. Taylor, R.P. Andres, W.N. Delgass, J. Phys. Chem. B 109 (2005) 2321.
[29] B. Taylor, J. Lauterbach, W.N. Delgass, Appl. Catal. A 291 (2005) 188.
[30] C. Qi, T. Akita, M. Okumura, K. Kuraoka, M. Haruta, Appl. Catal. A 253 (2003) 75.
[31] J.P. Dever, K.F. George, W.C. Hoffman, H. Soo, Ethylene Oxide, in: Kirk-Othmer: Encyclopedia of Chemical Technology, vol. 9, fourth ed., Wiley, New York, 1995, p. 915.
[32] A.S.K. Hashmi, G.J. Hutchings, Angew. Chem. Int. Ed. 45 (2006) 7896.
[33] D.H. Wells, W.N. Delgass, K.T. Thomson, J. Catal. 225 (2004) 69.
[34] J.Q. Lu, X. Zhang, J.J. Bravo-Suárez, S. Tsubota, J. Gaudet, S.T. Oyama, Catal. Today 123 (2007) 189.
[35] J.C. Jansen, Z. Shan, L. Marchese, W. Zhou, N. van der Puil, Th. Maschmeyer, Chem. Commun. 8 (2001) 713.
[36] S. Tsubota, D.A.H. Cunningham, Y. Bando, M. Haruta, Stud. Surf. Sci. Catal. 91 (1995) 227.
[37] T. Blasco, A. Corma, M.T. Navarro, J.P. Pariente, J. Catal. 156 (1995) 65.
[38] M.D. Alba, Z. Luan, J. Klinowski, J. Phys. Chem. 100 (1996) 2178.
[39] S. Gontier, A. Tuel, J. Catal. 157 (1995) 124.
[40] R.J. Davis, Z. Liu, Chem. Mater. 9 (1997) 2311.
[41] Z. Liu, G.M. Crrumbaugh, R.J. Davis, J. Catal. 159 (1996) 83.
[42] G. Mul, A. Zwijnenburg, B. Linden, M. Van der Makkee, J.A. Moulijn, J. Catal. 201 (2001) 128.
[43] R.E. Benfield, D. Grandjean, M. Kröll, R. Pugin, T. Sawitowski, G. Schmid, J. Phys. Chem. B 105 (2001) 1961.
[44] A. Fernandez, A. Caballero, A.R. Gonzalez-Elipe, J.-M. Herrmann, H. Dexpert, F. Villain, J. Phys. Chem. 99 (1995) 3303.
[45] T.M. Salama, T. Shido, R. Onishi, M. Ichikawa, J. Phys. Chem. 100 (1996) 3688.
[46] K.K. Bando, N. Ichikuni, K. Soga, K. Kunimori, H. Arakawa, K. Asakura, J. Catal. 194 (2000) 91.
[47] R.B. Greegor, F.W. Lytle, J. Catal. 63 (1980) 476.
[48] A.I. Frenkel, C.W. Hills, R.G. Nuzzo, J. Phys. Chem. B 105 (2001) 12689.
[49] G.C. Bond, D.T. Thompson, Catal. Rev. Sci. Eng. 41 (1999) 319.
[50] F. Moreau, G.C. Bond, A.O. Taylor, J. Catal. 231 (2005) 105.
[51] D.G. Barton, S.G. Podkolzin, J. Phys. Chem. B 109 (2005) 2262.
[52] D.A.H. Cunningham, W. Vogel, H. Kageyama, S. Tsubota, M. Haruta, J. Catal. 177 (1988) 1.
[53] Q. Fu, H. Saltburg, M. Flytzani-Stephanopoulous, Science 301 (2003) 935.
[54] M. Haruta, Gold Bull. (London, UK) 37 (2004) 27.
[55] L.M. Molina, M.D. Rasmussen, B. Hammer, J. Chem. Phys. 120 (2004) 7673.
[56] J.T. Miller, A.J. Kropf, Y. Zha, J.R. Regalbuto, L. Delannoy, C. Louis, E. Bus, J.A. van Bokhoven, J. Catal. 240 (2006) 222.
[57] J. Radnik, L. Wilde, M. Schneider, M.-M. Pohl, D. Herein, J. Phys. Chem. B 110 (2006) 23688.
[58] M. Okumura, S. Tsubota, M. Haruta, J. Mol. Catal. A Chem. 199 (2003) 73.
[59] C. Qi, T. Akita, M. Okumura, M. Haruta, Appl. Catal. A 218 (2001) 81.
[60] B. Chowdhury, J.J. Bravo-Suárez, N. Mimura, J.Q. Lu, K.K. Bando, S. Tsubota, M. Haruta, J. Phys. Chem. B 110 (2006) 22995.